

Aberystwyth University

Pulsed iceberg delivery driven by Sturtian ice sheet dynamics

Le Heron, Daniel P.; Busfield, Marie E.

Published in:
Sedimentology

DOI:
[10.1111/sed.12225](https://doi.org/10.1111/sed.12225)

Publication date:
2016

Citation for published version (APA):

Le Heron, D. P., & Busfield, M. E. (2016). Pulsed iceberg delivery driven by Sturtian ice sheet dynamics: An example from Death Valley, California. *Sedimentology*, 63(2), 331-349. <https://doi.org/10.1111/sed.12225>

General rights

Copyright and moral rights for the publications made accessible in the Aberystwyth Research Portal (the Institutional Repository) are retained by the authors and/or other copyright owners and it is a condition of accessing publications that users recognise and abide by the legal requirements associated with these rights.

- Users may download and print one copy of any publication from the Aberystwyth Research Portal for the purpose of private study or research.
- You may not further distribute the material or use it for any profit-making activity or commercial gain
- You may freely distribute the URL identifying the publication in the Aberystwyth Research Portal

Take down policy

If you believe that this document breaches copyright please contact us providing details, and we will remove access to the work immediately and investigate your claim.

tel: +44 1970 62 2400
email: is@aber.ac.uk

Pulsed iceberg delivery driven by Sturtian ice sheet dynamics: an example from Death Valley, California

DANIEL P. LE HERON & MARIE E. BUSFIELD

Department of Earth Sciences, Royal Holloway University of London, Egham, Surrey, TW20 0EX (e-mail: daniel.le-heron@rhul.ac.uk)

ABSTRACT

The Kingston Peak Formation is a Cryogenian sedimentary succession that crops out in the Death Valley area, California. It is widely accepted to record pre-glacial conditions (KP1), followed by two glaciations of pan-global extent, the older Sturtian (KP2-3) and younger Marinoan glaciation (KP4). In the type area (the Kingston Range), detailed facies analysis of the Sturtian succession reveals a basal diamictite unit and an upper boulder conglomerate were deposited by proglacial subaqueous sediment gravity flows. An olistostrome unit punctuating the succession is interpreted to result from tectonically-induced downslope mobilisation during isostatic rebound, triggered by significant ice-meltback. Focussing on strata onlapping the olistostrome, this paper provides insight into the processes of glacial re-advance following an intra-Sturtian glacial minimum. The first 50 m of strata above the olistostrome are thinly-bedded turbidites that are devoid of lonestones. A trend toward thicker graded beds upsection, in concert with the gradual appearance and then abundance of lonestones, testifies to the influence of ice rafting and to the resumption of a direct ice sheet influence upon sedimentation. Stratigraphic organisation into thickening and coarsening upward bedsets over a multi-metre scale reveals a subaqueous gravity flow-dominated succession composed of a spectrum of high to low density turbidites, with thick graded boulder-conglomerates at intervals. The finer-grained facies assemblage is heterolithic: current ripple cross-laminated sandstones intercalated with shales that bear delicate granule to pebble-sized dropstones in abundance. Intervals of dropstone-bearing and dropstone-free strata are attributable to dynamic oscillation of the ice margin in the hinterland. Integrating palaeocurrent data with observations from neighbouring outcrop belts allow a detailed palaeogeographic map of the eastern Death Valley area to be compiled for the first time.

32

33 INTRODUCTION

34 The Sturtian glaciation is the oldest of two major glacial intervals in the Cryogenian interval
35 and considered to span approximately 60 Ma (Rooney et al., 2014). In the Death Valley area,
36 California, lower to middle levels of the Kingston Peak Formation are renowned as an
37 excellent example of the interplay between extensional tectonics and glaciation (e.g. Basse,
38 1978; Miller, 1985; Link et al., 1993; Prave, 1999; Macdonald et al., 2013; Le Heron et al.,
39 2014), contributing to the debate on tectonic versus glaciogenic controls upon diamictites in
40 the Neoproterozoic on a global scale (Eyles and Januszczak, 2004). These deposits, of
41 interpreted Sturtian age (Prave, 1999) have thus received a resurgence of interest since the
42 early sedimentological models were developed (Basse, 1978; Miller, 1985), stemming
43 ultimately from the interest stirred by the snowball Earth hypothesis (Hoffman et al., 1998).
44 Neoproterozoic strata crop out in typically well-exposed but disconnected outcrop belts,
45 providing detailed insight into ice sheet dynamics in the southern Cordillera. Understanding
46 palaeo-ice sheet behaviour, via a detailed scrutiny of facies and stratigraphic architecture,
47 provides valuable boundary conditions for climate models in the Sturtian icehouse world
48 (Hyde et al., 2000; Pierrehumbert, 2005; Le Hir et al., 2007; Pierrehumbert et al., 2011).

49 In eastern California, the Kingston Peak Formation (**Fig. 1**) preserves an
50 exceptionally well exposed, thick, and laterally extensive succession that includes glaciogenic
51 strata of both early Cryogenian (Sturtian) and late Cryogenian (Marinoan) age (Macdonald et
52 al., 2013; Le Heron et al., 2014). This region, representing the type area of the Kingston Peak
53 Formation, demonstrates clear evidence for a glacial influence on sedimentation (e.g. Mrofka
54 & Kennedy, 2011; Macdonald et al., 2013), including major advance-retreat cycles (Le Heron
55 et al., 2014). In the northern Kingston Range, both Macdonald et al. (2013) and Le Heron et

56 al. (2014) described a >1 km thick olistostrome unit punctuating the Sturtian succession. This
57 interval has been interpreted as a glacial minimum (Le Heron et al., 2014), with retreat of the
58 ice front triggering isostatic rebound, tectonism, and unbuttressing of the carbonate bedrock.
59 These processes led to remobilisation of angular olistoliths downslope, accompanied by
60 background ice-rafting following widespread ice sheet disintegration. Above this horizon,
61 conglomerate and graded sandstone facies are interpreted to record subaqueous outwash
62 during a glacial re-advance (Le Heron et al., 2014). However, the contact between the
63 olistostrome unit and overlying strata is largely obscure in the northern Kingston Range
64 owing to the high proportion of muddy deposits that are typically recessive on hillsides.

65 This paper targets the southern Kingston Range (**Fig. 1**), where outstanding gully
66 sections permit the olistostrome and supra-olistostrome units to be clearly distinguished. In
67 contrast to other regions in the Death Valley area, mudstone-rich intervals are well exposed,
68 and demonstrate clear variations in the content of ice-rafted debris. The paper therefore aims
69 to: (1) document the facies associations preserved in the supra-olistostrome unit, (2) comment
70 on the distribution of ice-rafted debris (IRD) in the succession and its relation to ice sheet
71 dynamics and (3) assess the regional palaeogeography during deposition of part of the
72 Kingston Peak Formation, as a first step toward constraining the geometry of the palaeo-ice
73 margin.

74

75 **REGIONAL GEOLOGY AND STRATIGRAPHY**

76 In ascending order, the Pahrump Group traditionally comprises three subdivisions: the
77 Crystal Spring Formation, the Beck Spring dolomite, and the Kingston Peak Formation
78 (Prave, 1999; Macdonald et al., 2013). Recent detrital zircon ages constrain the upper Crystal
79 Spring Member to younger than 787 ± 11 Ma, which Mahon et al. (2014a) use to propose a

80 separate 'Horse Thief Springs Formation'. This offers a maximum depositional age for the
81 Kingston Peak Formation, which is recognised as older than 635 Ma based upon angular
82 truncation beneath the Noonday Dolomite (Pettersen et al., 2011; Macdonald et al., 2013). No
83 palaeomagnetic data are available from the Kingston Peak Formation itself, although Evans
84 (2000) obtained a near-equatorial ($01 \pm 4^\circ$) palaeolatitude from the Johnnie Formation some
85 hundreds of metres stratigraphically upsection.

86 The Kingston Peak Formation is considered to span two intracratonic rifting events,
87 associated with break-up of the supercontinent Rodinia (Prave, 1999; Mahon et al., 2014a). In
88 the southern Panamint Range, MORB-type pillow lavas are intercalated with diamictites
89 belonging to the lower part of the Kingston Peak Formation in Surprise Canyon (Labotka et
90 al., 1980; Miller, 1985). This key finding, taken together with evidence for "buried faults" led
91 Prave (1999) to propose an early phase of rifting at about 700 Ma. In the Kingston Range, in
92 the vicinity of Horsethief Spring, a series of spectacular en echelon normal faults, dissecting
93 the upper part of the Kingston Peak Formation can be observed on satellite imagery (Le
94 Heron, 2015).

95 A second phase of rifting during Kingston Peak times was proposed by Prave (1999)
96 at about 600 Ma on account of an olistostrome mapped in Goler Wash, southern Panamint
97 Range. This olistostrome, it was shown, progressively truncated underlying KPF strata down
98 to crystalline basement, and was itself capped by an upper diamictite termed the Wildrose
99 Diamictite (Miller, 1985). Elsewhere in the Death Valley area, olistostromes with km-scale
100 blocks occur in the central and southern Kingston Range (Macdonald et al., 2013; Le Heron
101 et al., 2014 & this paper). Large, angular blocks of dolostone derived from the Crystal Spring
102 Formation are mappable in the Silurian Hills (Kupfer, 1960) where crystalline basement
103 fragments are also common (Basse, 1978).

104 Evidence for olistostromes in the Pahrump Group is confined to the Kingston Peak
105 Formation. However, it is noted that arkosic sandstone and granular conglomerates-
106 presumably implying downcutting to crystalline basement- occur at intervals in other units,
107 notably in the Crystal Spring Formation (Macdonald et al., 2013). Carbonate conglomerate
108 intervals at the base of the Horse Thief Spring Formation record deposition following a 300
109 Ma duration hiatus (Mahon et al., 2014a). Regional zircon data suggest an evolution in
110 sediment routing systems, with provenance from the NE (Colorado) during latest Tonian and
111 early Cryogenian time, with progressive input from the SE and E into the Cryogenian
112 (Mahon et al., 2014b).

113 Macdonald et al. (2013) adopted and refined the regional allostratigraphy for the
114 Cryogenian Kingston Peak Formation developed by Prave (1999). In that framework, the
115 formation is subdivided into 4 units; KP1-4 in ascending stratigraphic order. Owing to the
116 lack of glacial indicators in the lower part of the formation, KP1 is considered to predate the
117 growth of ice sheets that deposited glaciogenic strata of KP2-4. In the Panamint Range, an
118 angular unconformity and package of non-glacial carbonate separates units KP3 and KP4,
119 leading to their interpretation as products of the older Sturtian and younger Marinoan
120 glaciation, respectively (Prave, 1999; Petterson et al., 2011). Le Heron et al. (2014) did not
121 find clear evidence for a KP4 unit in their study area in the northern Kingston Range,
122 although a detailed sedimentary model for units KP2-KP3 was developed in that paper. KP2
123 consisted entirely of a dropstone-bearing diamictic unit, but the olistostrome and supra-
124 olistostrome succession were restricted to unit KP3 (Le Heron et al., 2014).

125

126 **THE SOUTHERN KINGSTON RANGE**

127 High quality exposure of unit KP3 is recorded within a series of N-S oriented gulleys that
128 dissect the southern Kingston Range, providing the basis for both correlation (**Fig. 2**) and
129 high resolution facies analysis (**Fig. 3**) that underpin this paper. The contact between the
130 olistostrome and supra-olistostrome succession is well preserved and is sharply defined in the
131 field by a colour change from dark grey weathering, manganiferous deposits to light brown
132 strata (**Fig. 4A**). At the outcrop scale, the olistostrome succession bears very angular blocks
133 of dolostone of boulder size (**Fig. 4B**), extending to km-scale blocks in the northern Kingston
134 Range (Le Heron et al., 2014). This unit is succeeded by heterolithic facies of the supra-
135 olistostrome succession (**Fig. 4C**).

136 Five detailed sedimentary logs in this area, supplemented by additional data from the
137 northern Kingston Range, are presented herein. The location of logged sections is shown on
138 the geological map (**Fig. 1**). A correlation panel for the strata (**Fig. 2**) clearly demonstrates
139 that some beds can readily be traced (by carefully walking out the contacts in the field), but in
140 other cases, internal complexity is such that bed-by-bed correlation is sometimes impossible.
141 The logged sections are partly simplified, thus an expanded, maximum-detail log is presented
142 for the most important and continuous section (Log 2, **Fig. 3**). For ease of comparison, the
143 facies scheme developed for the northern Kingston Range (Le Heron et al., 2014) and Sperry
144 Wash (Busfield & Le Heron, 2015, this volume) will be adopted herein. Focussing on the
145 topmost unit in the succession (KP3), this study is restricted to three facies associations: 1)
146 Pebble to boulder conglomerate, 2) Interbedded heterolithics, and 3) Lonestone-bearing. This
147 locality is down palaeo-dip from the northern Kingston Range sections, evidenced in
148 measured palaeocurrent orientations, and is further reflected in downslope changes in facies
149 character, discussed below.

150

151 **Pebble to boulder conglomerate facies association**

152 *Description*

153 On the basis of grain size and matrix content, several subfacies are distinguished, namely
154 clast-supported cobble- to boulder-rich conglomerates, clast-supported granule- to pebble-
155 rich conglomerates, and matrix-supported conglomerates (**Fig. 2-3**). Clasts are dominated by
156 carbonates of the Crystal Spring and Beck Spring Dolomite, although sandstone intraclasts
157 are also recognised, and are typically sub-rounded to rounded. Where discoid clasts are
158 present, imbrication is developed in boulders at the base of beds. Stacked conglomeratic
159 bedsets which thicken upwards occur at intervals (e.g. 70 m, 80 m, 95 m, Log 1, **Fig. 2**).

160 Continuous intervals of cobble- to boulder-rich conglomerates extend up to 11 m in
161 thickness (e.g. **Fig. 2**, log 1, 57-68 m), but typically occur in beds 1-2 m thick (multiple
162 intervals in log 2, **Figs 2-3; Fig. 4 D**). These facies are predominantly normally-graded, with
163 sharp bed bases in all cases. Some deposits occur above irregular basal contacts, defining
164 lenticular lithosomes 5 m wide and 0.75 m in thickness (**Fig. 4D**). Granule- to pebble-rich
165 conglomerates share many of these characteristics with their coarser-grained counterparts, but
166 tend to occur as thinner (~0.5 m beds). Furthermore, although the cobble- to boulder-rich
167 conglomerates are rare, the granule- to pebble-rich varieties occur with greater regularity, and
168 over intervals of ≤ 5 m.

169 Matrix-supported conglomerates are comparatively rare, with bed thicknesses
170 typically < 30 cm, attaining clast-width in the case of boulder-bearing beds. In contrast to
171 their pebble to boulder-rich counterparts, these conglomerates are ungraded. Internally,
172 pebble-sized mud chips are observed, forming detached rootless folds in some instances (**Fig.**
173 **4 E**).

174

175 *Interpretation*

176 The clast-supported pebble to boulder conglomerates are interpreted as hyperconcentrated
177 flow deposits (massive) and high-density turbidites (normally-graded) (cf. Lowe, 1982;
178 Kneller, 1995; Mulder & Alexander, 2001; Winsemann et al., 2009; Talling et al., 2012).
179 High sediment concentrations within these flows act to dampen turbulence, and thus hinder
180 the development of bedforms (Talling et al., 2012). The transition from massive to normally-
181 graded varieties is interpreted to reflect flow transformation from moderate cohesive strength
182 debris flows to turbidity currents (Hampton, 1972, Tinterri et al., 2003; Amy & Talling,
183 2006; Talling et al., 2012). In this scenario, dilution and mixing with the overlying water
184 column during downslope remobilisation promotes increased turbulence and sorting, leading
185 to deposition of normally-graded beds. It is noteworthy that within the northern Kingston
186 Range, massive hyperconcentrated flows dominate (Le Heron et al., 2014), whereas
187 downslope in the southern Kingston Range more dilute, turbidites are far better developed.

188 Thickening-upwards conglomeratic bedsets are interpreted to record the build-up of
189 lobe elements, the constituent ‘building blocks’ of depositional lobes, which in turn stack to
190 form a lobe complex (Prélat et al., 2009; Macdonald et al., 2011). An axis to off-axis position
191 within the lobe complex is favoured by their coarse calibre and occurrence of amalgamated
192 bedsets (Prélat et al., 2009; Prélat & Hodgson, 2013). Stacked conglomeratic lobe elements
193 are commonly overlain by siltstones of the interbedded heterolithics facies association,
194 representing lobe switching/abandonment.

195 Matrix-supported conglomerates are interpreted as debris flows of a moderate
196 cohesive strength. Pebble-sized mud chips are interpreted as rip-up clasts incorporated from
197 underlying semi-lithified silt-grade sediments. Their chaotic orientation is consistent with

198 transport within a debris flow (Talling et al., 2012). The rarity of these debrites in the
199 succession of the southern Kingston Range is remarkable given that 6 km further north
200 abundant, matrix-supported conglomerates interpreted as glaciogenic debris flows (GDFs) are
201 preserved (Le Heron et al., 2014). This provides further credence that the southern Kingston
202 Range represents a more distal depositional setting. By analogy to Pleistocene glacier-fed
203 deep marine environments, these sediments are interpreted as elongate debrite lobes
204 interfingering with turbidites on the slope and into the basin plain (Escutia et al., 2000;
205 Taylor et al., 2002).

206

207 **Interbedded heterolithics facies association**

208 *Description*

209 This facies association comprises closely interbedded siltstones and thick-bedded, normally-
210 graded sandstones. They occur either as isolated beds punctuating siltstone facies, or as the
211 basal part of coarsening- and thickening-upward cycles that culminate in conglomerates (**Fig.**
212 **5A**). The sandstones exhibit classic sole mark structures at their bases, including flute marks
213 and grooves (**Fig. 5B**), and sharp to irregular bed bases (**Fig. 5C**). Composite cross-
214 laminations with climbing geometries are common. Additionally, flame structures occur at
215 the contact between sandstones and underlying siltstones, and convolute bedding locally
216 disrupts or obscures bed contacts. The graded sandstones occur with similar stratigraphic
217 regularity to their granule- to pebble-rich conglomerate counterparts. Two isolated examples
218 of ungraded sandstones with dune-scale cross-stratification are also recorded, at 25 m and 27
219 m in Log 1 (**Fig. 2**). The beds are sharp-based and bounded by siltstone facies.

220 Lonestone-free siltstones constitute approximately 40% of the succession by volume
221 studied in the southern Kingston Range. Intervals of thin-bedded and normally-graded
222 sandstones (2-10 cm thick) are intercalated with siltstone facies. Siltstone-dominated
223 intervals contain variable thicknesses of associated fine- to very fine-grained cross-laminated
224 sandstones. These are expressed as both laterally continuous sets and as laterally
225 disconnected to isolated lenses (**Figs. 5E, F**). Both morphologies exhibit principal palaeoflow
226 towards the SE. In vertical section, both cross-lamina co-sets and stratigraphically isolated
227 cross-lamina intervals occur. Some co-sets express climbing ripple cross-stratification (**Fig.**
228 **5E**). Piled load casts occur between superposed laminae, and flame structures occur at the
229 base of some of the thin sandstone intervals (**Fig. 5E**). Detached elliptical load-casts,
230 composed of individual cross-lamina lenses, are also preserved (**Fig. 5F**).

231

232 *Interpretation*

233 The majority of the thick-bedded sandstones are interpreted as T_A, T_{B-2} and T_C turbidites. The
234 exception may be the cross-stratified sandstones, since the generation of dune-scale cross-
235 stratification is rare in turbidites, possibly owing to the rapidity of sediment fallout
236 suppressing their development (Talling et al., 2012 and refs therein). They are therefore more
237 likely to originate through localised bottom-current reworking than from a primarily turbulent
238 process.

239 Within the dominant turbidite facies, the contact between T_{B-2} and T_C subdivisions is
240 characterised by a grain size break, recently summarised by Talling et al. (2012) as a
241 commonplace phenomenon in high density turbidites. However, ripple cross-laminated
242 intervals support fully turbulent conditions within low-density turbidity currents (T_C; Mulder
243 & Alexander, 2001; Baas et al., 2011; Talling et al., 2012). Cross-lamination with climbing

244 geometries also reflect fully turbulent conditions but under more rapid rates of sedimentation
245 (Baas, 2000; Kane & Hodgson, 2010; Jobe et al., 2012). The grain size break between T_{B-2}
246 and T_C subdivisions therefore probably records a bipartite structure to the flow in which
247 comparatively higher and lower sediment concentration layers become differentiated as the
248 flow evolves (Mutti, 1992; Mutti et al., 2003). Cross-laminated intervals are bounded by
249 planar laminated and massive siltstones, interpreted to record dilute, low-density turbidity
250 current deposits (T_D and T_{E-1} ; Talling et al., 2012), and hemipelagic fallout from the turbulent
251 suspension during waning flow (e.g. Allen et al., 2004). The range of ripple morphologies –
252 both as laterally continuous sets and isolated lenses – indicates fluctuations in sand supply in
253 the dilute turbidity currents, alongside elevated tractional re-working (e.g. Talling et al.,
254 2007, 2012). The piled load casts, detached elliptical load casts and flame structures originate
255 through density contrasts between rapidly deposited sand and underlying muds (Rayleigh-
256 Taylor instabilities; Allen, 1984). The thick, uninterrupted accumulations of this facies over
257 tens of metres are suggestive of continuous input of dilute sediment into the basin.

258

259 **Lonestone-bearing facies association**

260 *Description*

261 Lonestone-bearing strata constitute approximately 30% of the studied sections. Lithologically
262 the sediments are nearly identical to the lonestone-free siltstones of the interbedded
263 heterolithic facies association, comprising massive, laminated and ripple-cross laminated
264 siltstones and fine sandstones. Strata assigned to this facies association tend to exhibit
265 lonestones over dm-scale stratigraphic intervals: note that cm-thick, lonestone-free beds do
266 occur within these intervals. The following considers “outsize clasts” as granule-size and

267 larger were observed, i.e. the assignment was undertaken on the basis of macroscopic rather
268 than microscopic textures.

269 The lonestone-bearing heterolithics contain granule to boulder-sized lonestones
270 dominated by carbonate (both limestone and dolostone are represented), occasional siltstone
271 and arkose, and rarely quartzite. Clear flexure of underlying laminae beneath these lonestones
272 can be demonstrated (**Figs. 5G-H**). Most commonly, isolated clasts are found in the T_e
273 subdivision, but at some levels, clast clusters are observed. In a large number of cases,
274 puncturing and/or abrupt termination of laminae occurs against the margins of the clast, and
275 non-deformed strata overlie the lonestone.

276 It should be noted that the size of lonestones varies considerably upsection: the
277 greatest concentration of cobble- and boulder-sized clasts occurs toward the middle part of
278 Log 2 (52-80 m; **Fig. 3**). At this stratigraphic level, it is estimated that pebble- to cobble-
279 grade lonestones account for approximately 8-10% by stratal volume. Lonestone frequency is
280 considerably lower (2-6%) at most other stratigraphic levels. Rarely, concentrated intervals of
281 small lonestones (i.e. granules to small pebbles) occur over 2-3 cm stratigraphic intervals.
282 These thin belts of lonestones transcend clear-cut lithological boundaries in cm-thick graded
283 beds.

284 In vertical section, four examples of a switch between interbedded heterolithics to the
285 lonestone-bearing facies association are noted in our most complete section (**Fig. 2**).
286 Nevertheless, there are considerable lateral variations on this trend along strike. For example,
287 lonestone-bearing facies in log 2 (27-33 m, **Fig. 2**) correlate with lonestone-free sediments in
288 log 3 (7-10 m, **Fig. 2**). The basal section of Log 1 (**Fig. 2**), which based upon local
289 correlation is not preserved at the base of the other logged sections, demonstrates a notable
290 absence of lonestones.

291

292 *Interpretation*

293 The lonestone-bearing facies association, akin to comparable lonestone-free siltstones of the
294 interbedded heterolithic facies, are interpreted as the product of fully turbulent, low-density
295 turbidity currents. In this facies association, the deflected and pierced laminae beneath
296 lonestones, in concert with undeformed laminae that drape them, is strong evidence that they
297 are ice-rafted debris (IRD). Bouncing clasts in a turbulent suspension load has long been
298 predicted (Lowe, 1982), but this has not been reproduced experimentally (Talling et al.,
299 2012). Therefore, gravity flow processes should be dismissed as a possibility for forming the
300 dropstone textures. Moreover, dilute, low-density flows would not have the cohesive strength
301 to ‘raft’ up to boulder sized lonestones. Their presence within delicate ripple cross-laminated
302 siltstones and fine sandstones can only readily be explained by ice-rafting processes: other
303 mechanisms for the generation of dropstones (attached to the roots of trees, seaward rafting,
304 animal ingestion: Bennett et al., 1996) are clearly inappropriate for Cryogenian strata.

305 The lateral and vertical variability of IRD is remarkable. By transcending lithological
306 boundaries, the thin belts of granule- to small pebble-sized lonestones demonstrate that these
307 were also deposited as IRD. Surprisingly, perhaps, no occurrences of “trains” of granule-
308 grade lonestones (i.e. single-clast thick layers of material) are noted in the southern Kingston
309 Range which might point to local winnowing. Correlation between closely spaced sections
310 (**Fig. 2**) suggests that the absence of IRD in small, isolated sections should be treated with
311 caution, underscoring that multiple traverses are important to properly document the trends.
312 Clearly, the absence of IRD in a single section does not imply sedimentation free from glacial
313 influence. The 4 clear transitions from thin bedded heterolithics to lonestone-bearing facies
314 associations observed in the study section imply that IRD delivery to the basin was pulsed.

315 The potential mechanisms for this are considered in detail elsewhere (Le Heron, 2015). The
316 lateral correlation between lonestone-free and lonestone-bearing deposits may simply imply
317 that certain areas of the Southern Kingston Range escaped the influence of ice-rafted
318 material.

319 In summary, there appear to be caveats associated with the interpretation of an ice-
320 rafting influence based on lonestones. In addition, the approach does not account for the
321 mudstone fraction, and it has long been known that till pellets can be incorporated into fine-
322 grained rocks, providing more cryptic evidence of IRD. Till pellets are macroscopic,
323 typically rounded, grains of clay or diamicton in modern and Quaternary deposits (Cowan et
324 al., 2012). They have long been thought to form from suspended sediment in interstices
325 between melting ice crystals, developing in a range of supraglacial to subglacial
326 environments (Ovenshine, 1970). The problem is that texturally identical structures are
327 revealed as mudstone aggregates in fluvial settings (Gastaldo et al., 2013) implying that they
328 are not firmly diagnostic of ice-rafting.

329

330 **Lateral and vertical facies association distributions**

331 The studied sections preserve thick accumulations of thin bedded heterolithics, punctuated at
332 irregular intervals by conglomeratic beds which are typically thicker towards the north-west
333 and thin towards the south-east. The thickest conglomerate package (57-68 m Log 1, **Fig. 2**)
334 can be walked out laterally where it thins to 2 m (4-6 m Log 2, **Fig. 2**). This relationship both
335 demonstrates the extent of along-strike pinch out, and facilitates correlation between other
336 beds.

337 Upsection, a succession of stacked normally-graded conglomerates (88-102 m Log 1,
338 **Fig. 2**) correlates down-dip with a much more heterogeneous package of thinner
339 conglomerates and sandstones (32.5-59 m Log 2, **Fig. 2**), separated by lonestone-bearing and
340 lonestone-free heterolithics. Similarly, three conglomeratic beds above (117-125 m Log 1,
341 **Fig. 2**) thin over a distance of <100 m between logs 1 and 2, whereas siltstone and fine
342 sandstone packages typically thicken to the SE (**Fig. 2**). This is consistent with the regional
343 trend of successions thickening to the SE observed in the northern Kingston Range (Le Heron
344 et al., 2014), which in tandem with the strongly preferred palaeoflow to the SE (ripple
345 foresets: **Fig. 2**) supports a regional SE-dipping palaeoslope. The pinch out relationships of
346 the coarser facies are therefore interpreted to record proximal to distal thinning as sediment
347 fallout proceeds downslope.

348

349

350 **DISCUSSION**

351 **Palaeogeography**

352 There is a strong motivation for integrating data from the southern Kingston Range with that
353 from other outcrop belts across the Death Valley area into a regional context. Stratigraphic
354 frameworks have been developed by many other workers, and a detailed facies model has
355 been presented for the Panamint Range toward the west (Miller, 1985). To date, an integrated
356 sedimentological framework for the eastern Death Valley area has not hitherto been
357 proposed. As a first step toward such a model, integrating data from the southern Kingston
358 Range (present paper), the northern and central portions of the range (Le Heron et al., 2014),
359 Sperry Wash (Busfield and Le Heron, 2015, this volume) and the Silurian Hills (Kupfer,
360 1960; Basse, 1978) allows a gross depositional environments (palaeogeographic) map to be

361 proposed for the south-eastern Death Valley region (**Fig. 7**). This map should be regarded as
362 preliminary. When directional data from the south of the Kingston Range is integrated with
363 the evidence for systematic and consistent thickening from the northern to the southern part
364 of the range (Mrofka, 2010; Macdonald et al., 2013; Le Heron et al., 2014), strong evidence
365 emerges of a regional SE-dipping slope (**Fig. 7**). From this map view, the olistostrome is
366 interpreted to be restricted to a zone south of a NE-SW oriented growth fault system: this is
367 proven in the northern Kingston Range (Prave, 1999; Le Heron et al., 2014) yet speculative
368 north of the Silurian Hills (**Fig. 7**): basement clasts and angular dolostone blocks are mapped
369 in the Kingston Peak Formation in that area (Kupfer, 1960).

370 Owing to its palaeogeographic position, it is notable that strata in the southern
371 Kingston Range exhibit much more evidence of IRD than their northern counterparts.
372 Toward the northern part of the range, IRD is restricted to strata immediately between the
373 KP2 diamictite and the basal olistostome strata where they occur over a ca 15 m interval (Le
374 Heron et al., 2014). This underscores the importance of palaeogeographic position in the
375 recognition of IRD in Neoproterozoic strata, illustrating that in this case more proximal strata
376 allow a less compelling case for a dropstone influence to be made. In terms of gross facies
377 comparisons, sandy debrites are more commonplace in the northern Kingston Range (Le
378 Heron et al., 2014), whereas high density turbidites are the expression of the coarsest, thickest
379 beds in the interbedded heterolithics in the southern part of the range. This implies that
380 individual glaciogenic debris flow lobes either terminate in an intermediate zone or pass
381 distally into turbidites.

382 Some 50 km to the west of the southern Kingston Range, the Sperry Wash area is
383 proposed to have periodically occupied an ice-grounding line position, and a generally more
384 proximal position in the basin, during the deposition of unit KP3 (**Fig. 7**) (Busfield and Le
385 Heron, 2015, this volume). When integrated with the evidence for proximal-distal transition

386 from debrites to turbidites in the Kingston Range, it is proposed that the belt dominated by
387 debrite deposition is unlikely to have exceeded more than about 10 km width from proximal
388 to distal at the ice maximum (**Fig. 7**). The Sperry Wash outcrop belt also exhibits evidence
389 for a consistent SE-dipping palaeoslope, with almost identical palaeoflow orientations to the
390 southern Kingston Range (Busfield and Le Heron, 2015, this volume). On our
391 palaeogeographic map, note that we tentatively extend the E-W oriented ice margin to the
392 Saddle Peak Hills, where closely comparable graded beds, IRD-rich intervals, and intrabed
393 deformed zones to the Sperry Wash area can be observed.

394 Busfield and Le Heron (2015) suggest that the Sperry Wash area may have occupied a
395 fjord setting, hence implying that this part of the basin was fed by a valley glacier draining an
396 upland area to the north. Indeed, Wright et al. (1974) proposed that the area covered by our
397 map was divided into two upland regions during deposition of the Pahrump Group: the
398 Nopah Upland to the north of Sperry Wash and the Kingston Range, and the Mojave Upland
399 range immediately south of the present day Silurian Hills. In addition to the palaeocurrent
400 data herein and contained in Busfield and Le Heron (2015), further evidence for the presence
401 of highlands include the direct contact of the Noonday Dolomite onto gneissose basement at
402 the Gunsight Mine south of Tecopa (Mrofka, 2000).

403 In the model of Wright et al. (1974), regional slopes from the north and south fed
404 down into an E-W oriented basin (the Armargosa Basin). We adopt this configuration in our
405 preliminary palaeogeography, and propose two ice masses which we term the Mojave ice
406 sheet and the Nopah ice sheet. We also postulate the existence of a spur separating Sperry
407 Wash and Silurian Hills (**Fig. 7**). The reason for this is that whilst limestones in the Silurian
408 Hills are almost exclusively gneiss, schist and granite (Basse, 1978), none of these lithologies
409 have been observed in the Sperry Wash area, implying the presence of a physical barrier
410 preventing the drift of icebergs toward the north. Conversely, the Sperry Wash area records

411 no evidence for basement clasts akin to those recovered from the Silurian Hills (Busfield and
412 Le Heron, 2015, this volume). Noting that lateral offset between these two areas also
413 certainly occurred during the Cenozoic (Blakely et al. 1999), two credible hypotheses
414 emerge: (1) a silled basin or (2) a ridge of land to prevent the mixing of icebergs, and hence
415 IRD, between them. No data are currently available that allow these hypotheses to be tested.

416 Further afield, a substantial dataset was collected in the Panamint Range at the
417 western margin of Death Valley in the thesis work of Miller (1983). In the Panamints, the
418 Kingston Peak Formation has historically been divided into a series of members, including
419 the basal Limekiln Spring Member and overlying Surprise Member (Miller, 1985 and refs
420 therein). These rocks, which are overlain by a carbonate unit (Sourdough Limestone
421 Member), were argued to correspond to the first phase of rifting to affect the Death Valley
422 region in the Cryogenian (Prave, 1999), stratigraphically equivalent to units KP2 and KP3 in
423 the Kingston Range (Macdonald et al., 2013) and hence to the Sturtian glacial event. A fence
424 diagram and offlap relationships documented in Miller (1985) suggest a northward-dipping
425 basin margin in that region during this glaciation, including during emplacement of basalts
426 coeval with deposition of the Surprise Member.

427 Data from the Panamint Range, when considered alongside palaeocurrent data in **Fig.**
428 **7**, imply a complex regional basin configuration during deposition of the Sturtian-aged strata.
429 In summary, the data suggest two opposing regional palaeoslopes: a northward slope in the
430 Panamints (Miller, 1985) and in the Silurian Hills (Wright et al., 1974) and a south-eastward
431 slope in the Kingston Range / Sperry Wash area. Although regional rotation during Tertiary
432 transtension cannot be ruled out, , the regional data incorporating observations from the
433 Panamints strengthens the interpretation of two ice masses flowing in opposing directions to
434 the south (the Nopah ice sheet) and to the north (the Mohave ice sheet) (**Fig. 7**).

435

436 **Global implications**

437 Careful investigation of the Southern Kingston Range succession, together with neighbouring
438 outcrop belts in the Death Valley, illustrates that the strata exhibit strong evidence for
439 glaciomarine sedimentation in a proglacial basin. The predominance of turbidite deposits,
440 with well-expressed SE-directed palaeocurrents, are posited to have evolved from debrites
441 further north in the Kingston Range. Documenting the lateral and vertical distribution of IRD
442 in this region allows us to emphasise that (i) IRD has a complex lateral and vertical
443 distribution on a local scale in proglacial strata but in spite of this (ii) the record of ice rafting
444 is more clearly expressed at a distance of some tens of km from the palaeo-ice margin than in
445 more proximal settings. Our palaeogeographic map based on these data is the first detailed
446 attempt to do so in the eastern Death Valley area. Moreover, it allows a first order
447 interpretation of the location and orientation of the ice grounding zone when integrated from
448 data in Sperry Wash (Busfield and Le Heron, 2015, this volume). It is notable that grounding-
449 line wedges have been documented from other Cryogenian sedimentary records (Domack and
450 Hoffman, 2011), and their recognition is an important step in palaeogeographic
451 reconstruction.

452 Cryogenian glacial deposits continue to be viewed as deposits of snowball Earth
453 conditions (Hoffman et al., 1998) by much of the geological community, rather than deposits
454 of ice sheets exhibiting a near-identical sedimentary record to their Phanerozoic counterparts
455 (e.g. Etienne et al., 2007). Other interpretations such as a “slushball Earth” compromise
456 including the relative contributions of a high-tilt Earth and tectonic processes (see Fairchild
457 and Kennedy, 2007, for a review) are commonly sidelined. Papers attempting to quantify, via
458 numerical models, the magnitude of postglacial sea-level rise (Creveling and Mitrovica,

459 2014), to simulate the climate of Cryogenian glaciations (Feulner and Kienert, 2014), or
460 wishing to emphasise the significance of benthic macroscopic phototrophs (fossil finds) in
461 associated strata (Ye et al., 2015) all begin with the starting assumption of a snowball Earth
462 with a global, or near global ice cover. Predictions of the snowball Earth model stipulate
463 equatorial temperatures of -20°C (Hoffman and Schrag, 2002). However, sedimentological
464 evidence from the Marinoan glacial succession of South Australia reveals periglacial sand
465 wedges demonstrating an active regolith layer at the palaeotropics, and therefore mean
466 surface temperatures “within a few degrees of freezing” (Ewing et al., 2014).

467 In the Sturtian record, meanwhile, the Kingston Peak Formation does not support the
468 interpretation of a continuous ice cover, with transitions from ice contact to proglacial basins
469 envisaged. In concert with previous studies emphasising IRD abundance in Cryogenian strata
470 (Condon et al., 2002; Leather et al., 2002), or wave generated structures implying ice-free
471 areas (Allen and Etienne, 2008; Busfield and Le Heron, 2014), we envisage highly dynamic,
472 polythermal ice masses (Hambrey and Glasser, 2012). These ice masses exhibited multiple
473 advance and retreat cycles, releasing prodigious volumes of meltwater to explain repeatedly
474 stacked glaciogenic debris flows (in more proximal settings) and turbidites (in more distal
475 settings) in tandem with IRD. These characteristics strongly negate the requirement for
476 refugia or speculative polynyas to support “survivalist” ecosystems (e.g. Ye et al., 2015),
477 particularly as glacial minima conditions (Le Heron et al., 2014) and possible interglacials are
478 expected to yield open water conditions. In summary, the collection of basic sedimentological
479 datasets, to facilitate the compilation of palaeogeographic maps, remains fundamental to the
480 debate.

481

482 **CONCLUSIONS**

- 483 • In the southern part of the Kingston Range, a multi-km thick succession of the
484 Kingston Peak Formation includes an olistostrome succession and a supra-
485 olistostrome succession in unit KP3. In the central Kingston Range, the olistostrome
486 was interpreted as the deposits of a Sturtian glacial minimum, produced during an
487 isostatic rebound event prior to glacial re-advance (Le Heron et al., 2014). In the south
488 of the range, exceptional exposure quality allows detailed documentation of the supra-
489 olistostrome deposits via 5 high resolution sedimentary logs;
- 490 • The supra-olistostrome succession contains three facies associations. The pebble to
491 boulder conglomerate facies association records deposition from hyperconcentrated
492 flows to high density turbidity flows, ultimately debouched from the ice margin. The
493 heterolithic facies association is the more distal part of this system, deposited by more
494 dilute turbidity currents. The lonestone-bearing facies association, meanwhile,
495 additionally records the accumulation of ice-rafted debris in this underflow-dominated
496 proglacial setting;
- 497 • Consideration of the lateral relationship between facies illustrates that although the
498 thickest beds and intervals can be traced at outcrop over several hundreds of metres,
499 significant bed thinning does occur over several tens of metres. Together with
500 palaeocurrent data recovered from ripple cross-lamination, grooves and flutes casts, a
501 pronounced SE-directed slope is identified;
- 502 • A preliminary palaeogeographic map of the eastern Death Valley area interprets a
503 consistent SE-directed palaeoslope that included all parts of the Kingston Range and
504 the Sperry Wash area. An ice mass grounded in the latter area released efflux as
505 glaciogenic debris flows into the basin, forming a conglomerate-rich apron about 10
506 km in extent from proximal to distal. Beyond this zone, turbidite deposition was
507 dominant, and IRD is well preserved.

508

509 Acknowledgements: this work was part-supported by the Geological Society of London
510 Fermor Fund. This paper is dedicated to Tony Prave to whom the authors are indebted for his
511 general advice, and discussions in the field in an earlier field season which led to our 2014
512 paper from an earlier phase of work. We are grateful to the chief editor, Nigel Mountney, for
513 his patience, to three anonymous reviewers, and to Julian Dowdeswell for his thoughts on the
514 manuscript. This led to a much improved paper.

515

516 REFERENCES

- 517 **Allen, J.R.L.** (1984) *Sedimentary Structures: Their Character and Physical Basis*, volumes I
518 and II. Elsevier, Amsterdam.
- 519 **Allen, P.A. and Etienne, J.L.** (2008) Sedimentary challenge to snowball Earth. *Nature*
520 *Geoscience*, **1**, 817–825.
- 521 **Amy, L. and Talling, P.J.** (2006) Anatomy of turbidite and debrite sandstones based on long
522 distance (120 x 35 km) bed correlation, Marnoso-arenacea Formation, Northern
523 Apennines, Italy. *Sedimentology*, **53**, 161–212.
- 524 **Baas, J.H.** (2000) Duration of deposition from decelerating high-density turbidity currents.
525 *Sed. Geol.*, **136**, 71–88.
- 526 **Baas, J.H., Best, J.L. and Peakall, J.** (2011) Depositional processes, bedform development
527 and hybrid flows in rapidly decelerated cohesive (mud-sand) sediment flows.
528 *Sedimentology*, **58**, 1953–1987.
- 529 **Basse, R.A.** (1978) Stratigraphy, Sedimentology and Depositional Setting of the Late
530 Precambrian Pahrump Group, Silurian Hills, California. MS Thesis, Stanford University,
531 86p.
- 532 **Bennett, M.R., Doyle, P. and Mather, A.E.** (1996) Dropstones: their origin and significance.
533 *Palaeogeography Palaeoclimatology Palaeoecology*, **121**, 31–339.
- 534 **Blakely, R.J., Jachens, R.C., Calzia, J.P. and Langenheim, V.E.** (1999). Cenozoic basins
535 of the Death Valley extended terrane as reflected in regional-scale gravity anomalies. In:
536 Wright, L.A. & Troxel, B.W. (eds.): *Cenozoic Basins of the Death Valley Region*.
537 Boulder, Colorado, Geological Society of America Special Paper 333.
- 538 **Busfield, M.E. and Le Heron, D.P.** (2014). Sequencing the Sturtian icehouse: dynamic ice
539 behaviour in South Australia. *Journal of the Geological Society of London*, **171**, 443-456.
- 540 **Busfield, M.E. and Le Heron, D.P.** (2015, this volume) A Neoproterozoic ice advance
541 sequence, Sperry Wash, California. *Sedimentology*.

- 542 **Condon, D.J., Prave, A.R. and Benn, D.I. 2002.** Neoproterozoic glacial-rainout intervals:
543 Observations and implications. *Geology*, **30**, 35-38.
- 544 **Cowan, E.A., Christofferson, P. and Powell, R.D. (2012)** Sedimentological Signature of A
545 Deformable Bed Preserved Beneath An Ice Stream In A Late Pleistocene Glacial Sequence,
546 Ross Sea, Antarctica. *Journal of Sedimentary Research*, **82**, 270–282.
- 547 **Creveling, J.R. and Mitrovica, J.X. (2014)** The sea-level fingerprint of a Snowball Earth
548 deglaciation. *Earth and Planetary Science Letters*, **399**, 74-85.
- 549 **Domack, E.W. and Hoffman, P.F. (2011)** An ice grounding-line wedge from the Ghaub
550 glaciation (635 Ma) on the distal foreslope of the Otavi carbonate platform, Namibia, and
551 its bearing on the snowball Earth hypothesis. *Geol. Soc. Am. Bull.*, **123**, 1448-1477.
- 552 **Escutia, C., Eittreim, S.L., Cooper, A.K. and Nelson, C.H. (2000)** Morphology and
553 acoustic character of the Antarctic Wilkes Land turbidite systems: icesheet- sourced versus
554 river-sourced fans. *Journal of Sedimentary Research*, **70**, 84-93.
555
- 556 **Etienne, J.L., Allen, P.A., Rieu, R. and Le Guerroue, E. (2007)** Neoproterozoic glaciated
557 basins: a critical review of the Snowball Earth hypothesis by comparison with Phanerozoic
558 glaciations, in: Hambrey, M.J., Christoffersen, P., Glasser, N.F., Hubbard, B. (Eds.), *Glacial*
559 *Processes and Products*. International Association of Sedimentologists, Special
560 Publications, 436 pp.
561
- 562 **Evans, D.A.D. (2000)** Stratigraphic, geochronological, and paleomagnetic constraints upon
563 the Neoproterozoic climatic paradox. *American Journal of Science*, **300**, 347-433.
- 564 **Ewing, R.C., Eisenman, I., Lamb, M.P., Poppick, L., Maloof, A.C. and Fischer, W.W.**
565 (2014) New constraints on equatorial temperatures during a late Neoproterozoic snowball
566 Earth glaciation. *Earth and Planetary Science Letters*, **406**, 110-122.
- 567 **Eyles, N. and Januszczak, N. (2004)** ‘Zipper-rift’: a tectonic model for Neoproterozoic
568 glaciations during the breakup of Rodinia after 750 Ma. *Earth Science Reviews*, **65**, 1–73.
- 569 **Fairchild, I.J. and Kennedy, M.J. (2007)** Neoproterozoic glaciation in the Earth System.
570 *Journal of the Geological Society of London*, **164**, 895–921.
- 571 **Feulner, G. and Kienert, H. (2014)** Climate simulations of Neoproterozoic Snowball Earth
572 events; similar critical carbon dioxide levels for the Sturtian and Marinoan glaciations.
573 *Earth and Planetary Science Letters*, **404**, 200-205.
- 574 **Gastaldo, R.A., Pludow, B.A. and Neveling, J. (2013)** Mud Aggregates from the Katberg
575 Formation, South Africa: Additional Evidence for Early Triassic Degradational
576 Landscapes. *Journal of Sedimentary Research*, **83**, 531-540.
- 577 **Hambrey, M.J. and Glasser, N.F. (2012)** Discriminating glacier thermal and dynamic
578 regimes in the sedimentary record. *Sedimentary Geology*, **251**, 1-33.

- 579 **Hampton, M.A.** (1972) The role of subaqueous debris flow in generating turbidity currents.
580 *J. Sed. Petrol.*, **42**, 775–793.
- 581 **Hoffman, P.F.** and **Schrag, D.P.** (2002) The snowball Earth hypothesis: testing the limits of
582 global change. *Terra Nova*, **14**, 129-155.
- 583 **Hoffman, P.F., Kaufman, A.J., Halverson, G.P.** and **Schrag, D.P.** (1998) A
584 Neoproterozoic Snowball Earth. *Science*, **281**, 1342-1346.
- 585 **Hyde, W.T., Crowley, T.J., Baum, S.K.** and **Peltier, R.** (2000) Neoproterozoic 'snowball
586 Earth' simulations with a coupled climate/ice-sheet model. *Nature*, **405**, 425–429.
- 587 **Jobe, Z.R., Lowe, D.R.** and **Morris, W.R.** (2012) Climbing-ripple successions in turbidite
588 systems: depositional environments, sedimentation rates and accumulation times.
589 *Sedimentology*, **59**, 867–898.
- 590 **Kane, I.A.** and **Hodgson, D.** (2010) Submarine channel levees: criteria for recognition of
591 levee subenvironments: exhumed examples from The Rosario Fm (Baja, Mexico) and the
592 Laingsburg Fm. (Karoo Basin). *Mar. Petrol. Geol.*, **28**, 807–823.
- 593 **Kneller, B. C.** (1995) Beyond the turbidite paradigm: physical models for deposition of
594 turbidites and their implications for reservoir potential. *In: Characterization of Deep Marine*
595 *Systems* (Eds A.J. Hartley and D.J. Prosser), *Geol. Soc. Spec. Publ.*, **94**, 31–49.
- 596 **Kupfer, D.H.** (1960) Thrust faulting and chaos structure, Silurian Hills, San Bernadino
597 County, California. *GSA Bulletin*, **71**, 181-214.
- 598 **Labotka, T.C., Albee, A.L., Lanphere, M.A.** and **McDowell, S.D.** (1980) Stratigraphy,
599 structure and metamorphism in the central Panamint Mountains (Telescope Peak
600 quadrangle), Death Valley area, California, *Geological Society of America Bulletin*, **91**,
601 843–933.
- 602 **Leather, J., Allen, P.A., Brasier, M.D.** and **Cozzi, A.** (2002) Neoproterozoic snowball Earth
603 under scrutiny: Evidence from the Fiq glaciation of Oman. *Geology*, **30**, 891–894.
- 604 **Link, P.K., Miller, J.M.G.** and **Christie-Blick, N.** (1993) Glacial-marine facies in a
605 continental rift environment: Neoproterozoic rocks of the western United States Cordillera.
606 *In: Deynoux, M., Miller, J.M.G., Domack, E.W., Eyles, N., Fairchild, I.J., Young, G.M.*
607 *(Eds.), Earth's Glacial Record.* Cambridge Univ. Press, Cambridge, 29– 46.
- 608 **Le Heron, D.P.** (2015) The significance of ice-rafted debris in Sturtian glacial successions.
609 *Sedimentary Geology*, **322**, 19-33.
- 610 **Le Heron, D.P., Busfield, M.E.** and **Prave, A.R.** (2014) Neoproterozoic ice sheets and
611 olistoliths: multiple glacial cycles in the Kingston Peak Formation, California. *Journal of*
612 *the Geological Society, London*, doi: 10.1144/jgs2013-130

- 613 **Le Hir, G., Ramstein, G., Donnadiou, Y. and Pierrehumbert, R.T.** (2007) Investigating
614 plausible mechanisms to trigger a deglaciation from a hard Snowball Earth, *C. R. Geosci.*
615 **339**, 274–287.
- 616 **Lowe, D.R.** (1982) Sediment gravity flows: II. Depositional models with special reference to
617 the deposits of high-density turbidity currents. *J. Sed. Petrol.*, **52**, 279-297.
- 618 **Macdonald, F.A., Prave, A.R., Petterson, R., Smith, E.F., Pruss, S.B., Oates, K.,**
619 **Trotzok, D. and Fallick, A.E.** (2013) The Laurentian record of Neoproterozoic glaciation,
620 tectonism, and eukaryotic evolution in Death Valley, California. *Geological Society of*
621 *America Bulletin*, doi: 10.1130/B30789.1
- 622 **Mahon, R.C., Dehler, C.M., Link, P.K., Karlstrom, K.E. and Gehrels, G.E.** (2014a)
623 geochronologic and stratigraphic constraints on the Mesoproterozoic and Neoproterozoic
624 Pahrump Group, Death Valley, California: A record of the assembly, stability, and
625 breakup of Rodinia. *Geological Society of America Bulletin*, **126**, 652-664.
- 626 **Mahon, R.C., Dehler, C.M., Link, P.K., Karlstrom, K.E. and Gehrels, G.E.** (2014b)
627 detrital zircon provenance and paleogeography of the Pahrump Group and overlying
628 strata, Death Valley, California. *Precambrian Research*, **251**, 102-117.
- 629 **Miller, J.M.G.** (1983) Stratigraphy and sedimentology of the upper Proterozoic Kingston
630 Peak Formation, Panamint Range, eastern California. PhD Thesis, Santa Barbara,
631 California, University of California, 335 pp.
- 632 **Miller, J.M.G.** (1985) Glacial and syntectonic sedimentation: The upper Proterozoic
633 Kingston Peak Formation, southern Panamint Range, eastern California. *Geological*
634 *Society of America Bulletin*, **96**, 1537-1553.
- 635 **Mrofka, D.** (2010) Competing models for the timing of Cryogenian Glaciation: Evidence
636 from the Kingston Peak Formation, southeastern California. PhD dissertation, University
637 of California, Riverside.
- 638 **Mrofka, D. and Kennedy, M.** (2011) The Kingston Peak Formation in the eastern Death
639 Valley region. In: *The Geological Record of Neoproterozoic Glaciations* (Eds E. Arnaud,
640 G.P. Halverson and G. Shields-Zhou). Geological Society, London, Memoirs, **36**, 449-
641 458.
- 642 **Mulder, T. and Alexander, A.** (2001) The physical character of subaqueous sedimentary
643 density flows and their deposits. *Sedimentology*, **48**, 269–299.
- 644 **Mutti, E.** (1992) Turbidite Sandstones. Istituto di Geologia Universita di Parma & AGIP,
645 San Donato Milanese, 275 pp.
- 646 **Mutti, E., Tinterri, R., Benevelli, G., diBase, D. and Cavanna, G.** (2003) Deltaic, mixed
647 and turbidite sedimentation of ancient foreland basins. *Mar. Petrol. Geol.*, **20**, 733–755.

- 648 **Ovenshine, A.T.** (1970) Observations of iceberg rafting in Glacier Bay, Alaska, and the
649 identification of ancient ice-rafted deposits. *Geological Society of America Bulletin*, **81**,
650 891-894.
- 651 **Petterson, R., Prave, A.R. and Wernicke, B.P.** (2011) Glaciogenic and related strata of the
652 Neoproterozoic Kingston Peak Formation in the Panamint Range, Death Valley region,
653 California. In: *The Geological Record of Neoproterozoic Glaciations* (Eds E. Arnaud, G.P.
654 Halverson and G. Shields-Zhou). Geological Society, London, Memoirs, **36**, 449-458.
- 655 **Pierrehumbert, R.T.** (2005) Climate dynamics of a hard snowball Earth. *J. Geophys Res --*
656 *Atmospheres*. 110(D1) D01111 doi:10.1029/2004JD005162
- 657 **Pierrehumbert, R.T., Abbot, D., Voight, A. and Koll, D.** (2011) Neoproterozoic Climate.
658 *Annual Reviews of Earth and Planetary Sciences*, **39**, 417–60.
- 659 **Prave, A.R.** (1999) Two diamictites, two cap carbonates, two $\delta^{13}\text{C}$ excursions, two rifts: the
660 Neoproterozoic Kingston Peak Formation, Death Valley, California. *Geology*, **27**, 339-
661 324.
- 662 **Prélat, A. and Hodgson, D.M.** (2013) The full range of turbidite bed thickness patterns in
663 submarine lobes: controls and implications. *Journal of the Geological Society*, **170**, 209-
664 214.
- 665 **Prélat, A., Covault, J.A., Hodgson, D.M., Fildani, A. and Flint, S.S.** (2010) Intrinsic
666 controls on the range of volumes, morphologies, and dimensions of submarine lobes.
667 *Sedimentary Geology*, **232**, 66-76.
- 668 **Rooney, A.D., Macdonald, F.A., Strauss, J.V., Dudás, F. Ö., Hallmann, C. and Selby, D.**
669 (2014) Re-Os Geochronology and coupled Os-Sr isotope constraints on the Sturtian
670 snowball Earth. *Proceedings of the National Academy of Sciences*, **111**, 51-56.
- 671 **Talling, P.J., Amy, L.A., Wynn, R.B., Blackbourn, G. and Gibson, O.** (2007) Turbidity
672 current evolution deduced from extensive thin turbidites: Marnoso-arenacea Formation
673 (Miocene), Italian Apennines. *J. Sed. Res.*, **77**, 172–196.
- 674 **Talling, P.J., Masson, D.G., Sumner, E.J. and Malgesini, G.** (2012) Subaqueous sediment
675 density flows: Depositional processes and deposit types. *Sedimentology*, **59**, 1937–2003.
- 676 **Taylor, J., Dowdeswell, J.A., Kenyon, N.H. and O’Cofaigh, C.** (2002) Late Quaternary
677 architecture of trough-mouth fans: debris flows and suspended sediments on the
678 Norwegian margin. In: *Glacier-Influenced Sedimentation on High-Latitude Continental*
679 *Margins* (Eds J.A. Dowdeswell and C. O’Cofaigh), *Geol. Soc. London Spec. Publ.*, **203**,
680 55–71.
- 681 **Tinterri, R., Drago, M., Consomi, A., Davoli, G. and Mutti, E.** (2003) Modelling
682 subaqueous bipartite sediment gravity flows on the basis of outcrop constraints: first results.
683 *Mar. Pet. Geol.*, **20**, 911–933.

- 684 **Winsemann, J., Hornung, J.J., Meinsen, J., Bußmann, M. and Weber, C. (2009)**
685 Anatomy of a subaqueous ice-contact fan and delta complex, Middle Pleistocene, North-
686 west Germany. *Sedimentology*, **56**, 1041-1076.
- 687 **Wright, L.A., Troxel, B.W., Williams, E.G., Roberts, M.T. and Diehl, P.E. (1974)**
688 Precambrian sedimentary environments of the Death Valley region, eastern California and
689 Nevada. In: *Geological Society of America, Guidebook: Death Valley region, California*
690 *and Nevada* [prepared for the 70th Annual Meeting of Cordilleran Section, Geological
691 Society of America]. The Death Valley Publishing Company, Shoshone, CA, 27–35.
- 692 **Ye, Q., Tong, J., Xiao, S., Zhu, S., An, Z., Tian, L. and Hu, J. (2015)** The survival of
693 benthic macroscopic phototrophs on a Neoproterozoic snowball Earth. *Geology*, **43**, 507-
694 510.

695

696

697

698 **Figure captions**

699 *Figure 1.* Overview map of the main outcrops of Neoproterozoic strata in Death Valley. B:
700 Satellite image of the southernmost part of the Kingston Range (see A for location). C:
701 Simple geological map of the southern Kingston Range, covering the same geographic area
702 as the satellite image (B). The colour scheme matches that of Le Heron et al. (2014) for
703 comparison with strata further north in the range. Shown on this map are the locations of
704 detailed sedimentary logs which are presented in Figure 2.

705

706 *Figure 2:* Sedimentary logs corresponding to each of the locations that are shown in Fig. 1 C.
707 Note that three facies associations are recognised in this study. Three lines of evidence for a
708 SE-dipping, major palaeoslope can be established: (1), palaeocurrents in the rose diagram,
709 showing regional-dip corrected cross-laminations plus flute casts and grooves; (2), consistent
710 thinning and pinch out of the conglomerates on each of the logs in the same direction; (3),

711 based on previous evidence (Le Heron et al., 2014), thickening of the entire Kingston Peak
712 Formation away from growth faults in the Horsethief Spring area to the NW. On the logs,
713 note the clear alternation/ differentiation of lonestone-bearing and lonestone-free thin bedded
714 heterolithic deposits.

715

716 *Figure 3:* Expanded version of logged section 2 (Fig. 2) at a higher resolution, without
717 simplification, illustrating the vertical facies transitions at maximum-level detail. This log is a
718 key section owing to almost continuous exposure of the finer-grained fraction in water-
719 washed gullies, enabling the presence and absence of ice-rafted debris (IRD) to be
720 documented to a high level of confidence.

721

722 *Figure 4:* Macroscale phenomena. A: landscape-scale view of the contact between the top of
723 the olistostrome complex in KP3 and the base of the supra-olistostrome succession (see also
724 Fig. 1 C). B: Olistostrome complex at the outcrop scale, with extremely angular blocks of
725 dolostone embedded with a manganese-rich matrix. Kilometre-scale dolostone blocks also
726 occur at intervals (Fig. 1 C). C: View of the basal part of the supra-olistostrome complex,
727 characterised by well stratified interbedded sandstones, conglomerates, and heterolithic strata
728 (documented in Fig. 2, log 1, 0-55 m). D: Typical view of a series of thickly-bedded
729 sandstones (next to geologist in view) sharply overlain by a graded conglomerate bed (124 m,
730 log 1, Fig. 2). E: Top of a thickening-up, coarsening upward interval (87 m log 2; Figs. 2 &
731 3), culminating in a normally-graded conglomerate unit.

732

733 *Figure 5: Mesoscale phenomena. A: Flute casts indicating SE flow. B: Classic T_{A-C} cycle.*
734 Note the characteristic sharp grain-size break between the parallel laminated T_B interval and
735 the ripple cross-laminated T_C subdivision. C: Intercalated graded sandstone beds and
736 lonestone-bearing shales (arrowed). D: Climbing ripple sets, starved ripple lenses, and shale
737 laminae. Load clasts occur beneath the sandstone intervals. E: 2 m along strike from image in
738 D, showing a small dolostone granule with classic impact structure (hence a dropstone)
739 beneath. F: Pebble-sized dropstone, clearing puncturing a cm-thick graded bed. G: Boulder-
740 sized dropstone, typical of the interval 55-80 m in log 2. H: Matrix supported, muddy
741 conglomerate with detached, rootless, recumbent fold within the bed. Scales: Hammer is 32
742 cm long, coin is 1.9 cm diameter.

743

744 *Figure 6: Summary depositional model for the supra-olistostrome interval. Following a*
745 *glacial minimum (A), when the olistostrome was emplaced, ice sheets repopulated highlands.*
746 *Uplands were a source area for both the olistostrome and supra-olistostrome gravity flow*
747 *deposits. During glacial re-advance (B), icebergs delivered debris-laden material to the ice*
748 *front. A fairly constant meltwater supply was maintained to generate repetitively stacked*
749 *gravity flow deposits, and icebergs shed IRD. (C) Dynamic oscillation of the grounding line*
750 *in the hinterland, in this case minor recession and cessation of iceberg calving, halted the*
751 *delivery of IRD. Meanwhile, gravity flows continued to deliver sediment to the basin.*

752

753 *Figure 7: Gross depositional environments (palaeogeographic) sketch map of the Death*
754 *Valley area during Kingston Peak times, showing the posited location of the ice front over*
755 *Sperry Wash (see Busfield and Le Heron, this volume), with the southern Kingston Range*
756 *representing a comparatively ice-distal location. The southern Kingston Range received thick*

757 accumulations of turbidites and, less commonly, debrites ultimately derived from the ice
758 margin located toward the NW.

759

760

761

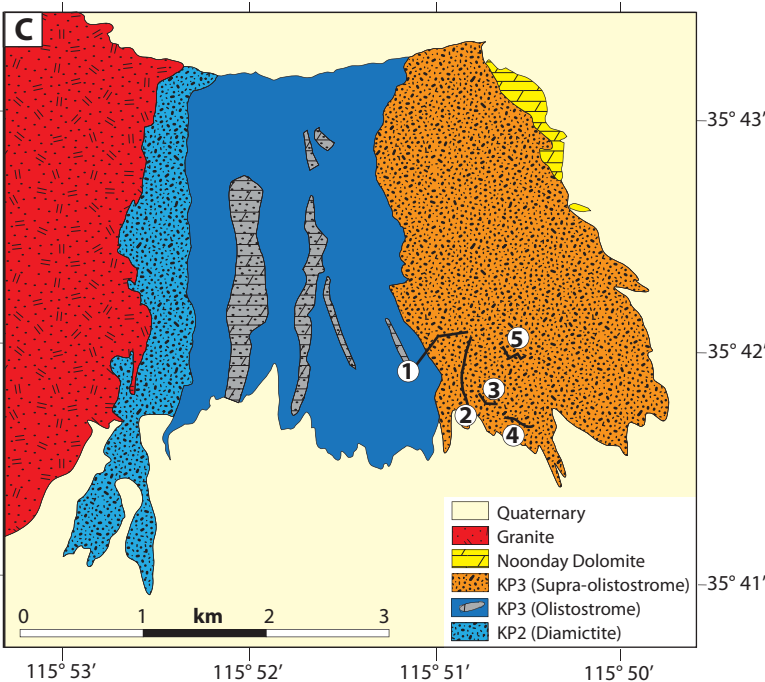
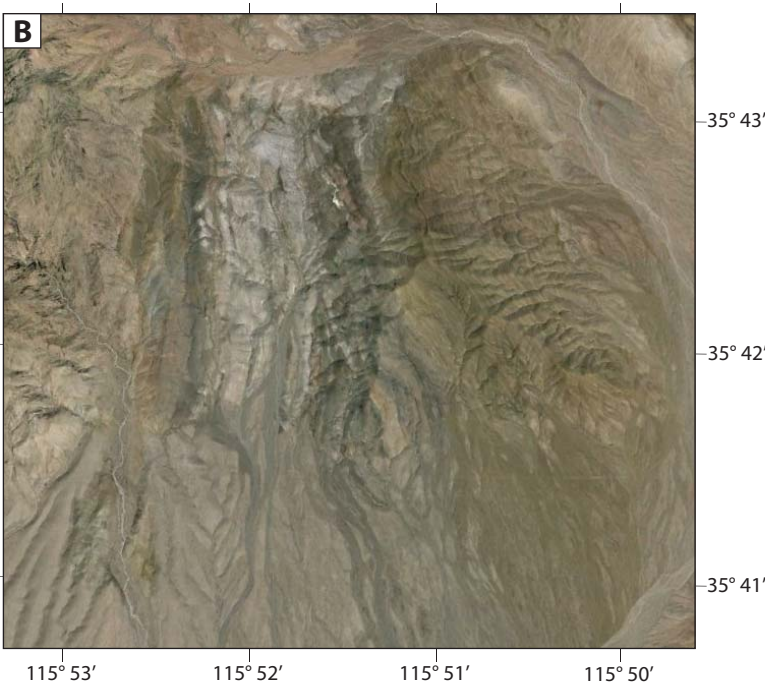
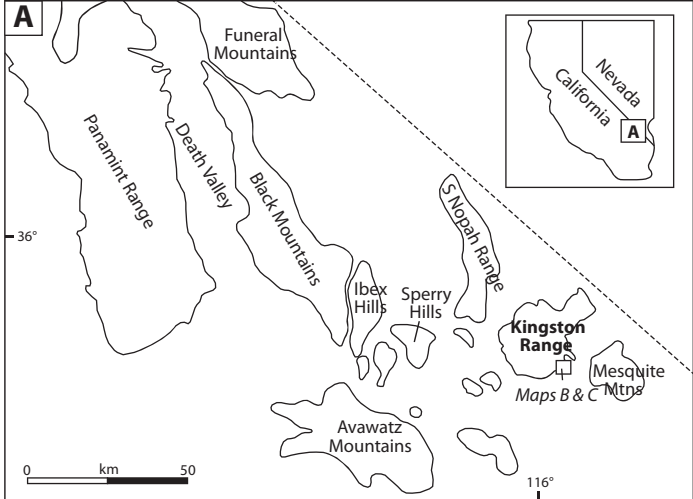


Figure 1

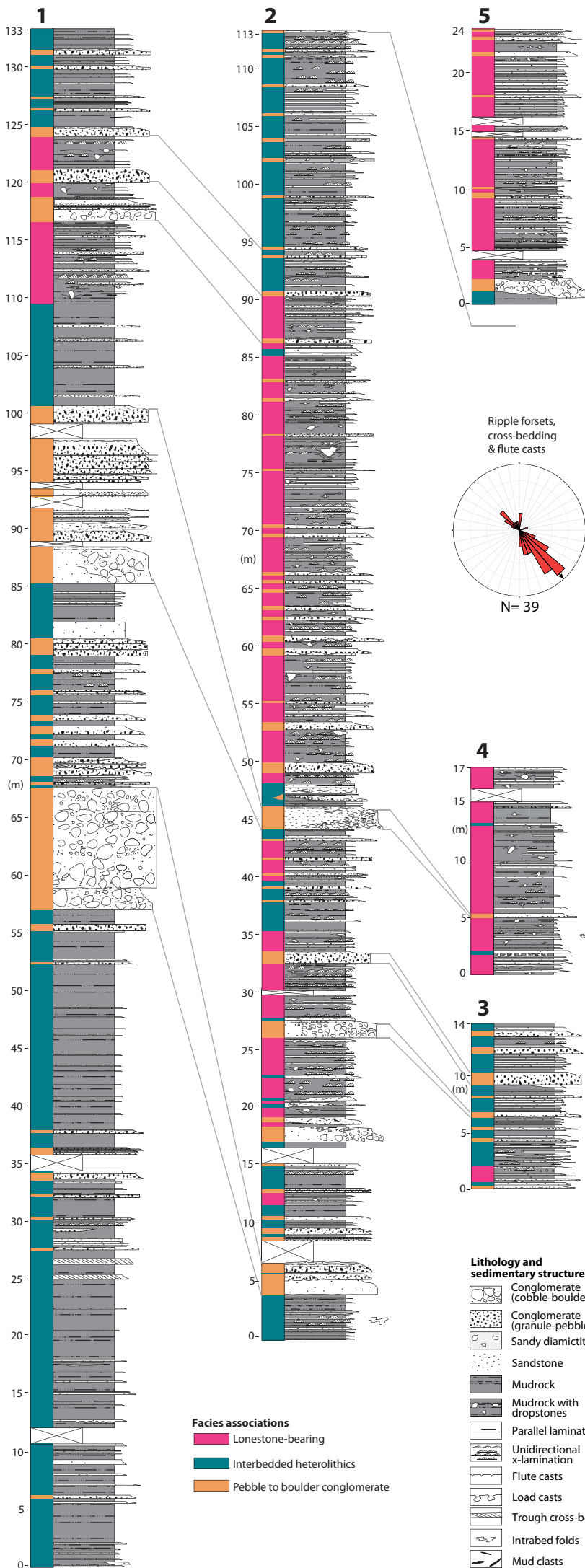
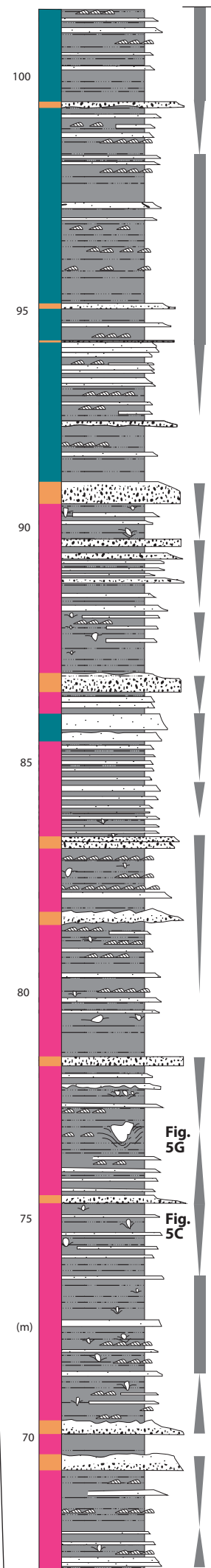
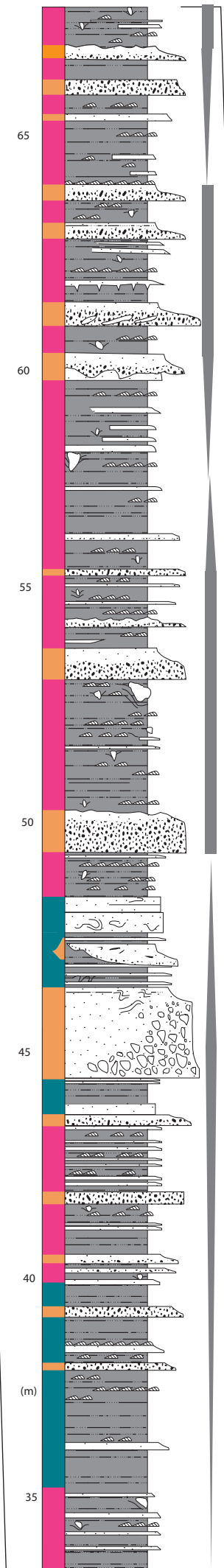
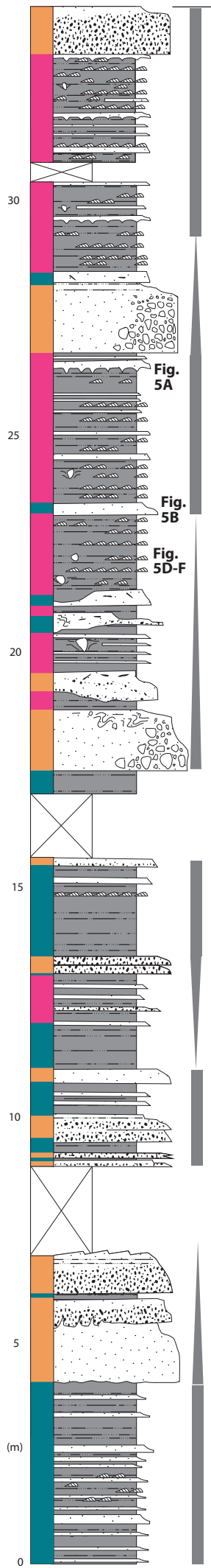


Figure 2



- Facies associations**
- Lonestone-bearing
 - Interbedded heterolithics
 - Pebble to boulder conglomerate
- Lithology and sedimentary structures**
- Conglomerate (cobble-boulder)
 - Conglomerate (granule-pebble)
 - Sandy diamictite
 - Sandstone
 - Mudrock
 - Mudrock with dropstones
 - Parallel lamination
 - Unidirectional x-lamination
 - Flute casts
 - Load casts
 - Trough cross-bedding
 - Intrabed folds
 - Mud clasts
- Grading patterns**
- ▲ Retrograding
 - Aggrading
 - ▼ Prograding

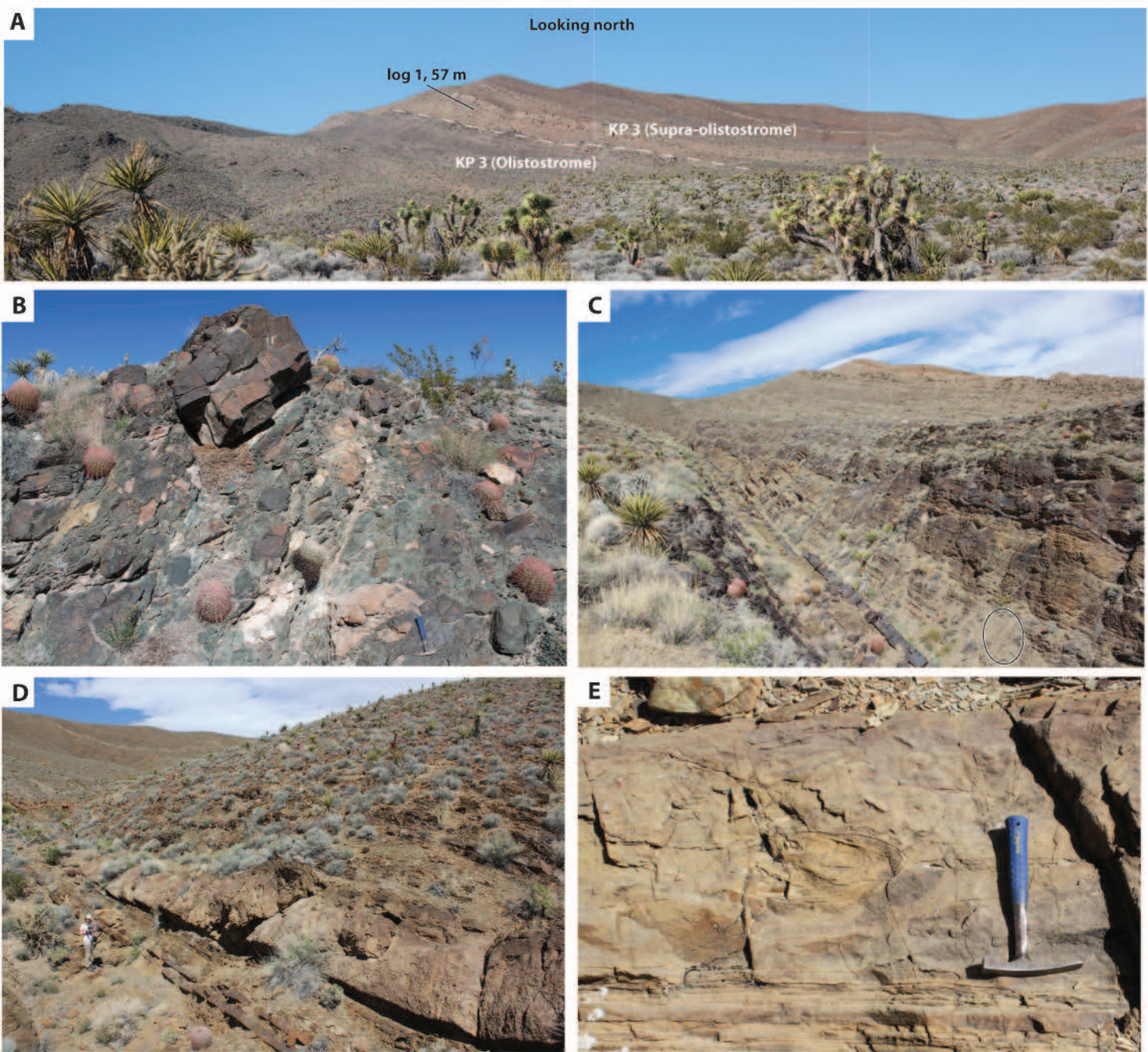


Figure 4

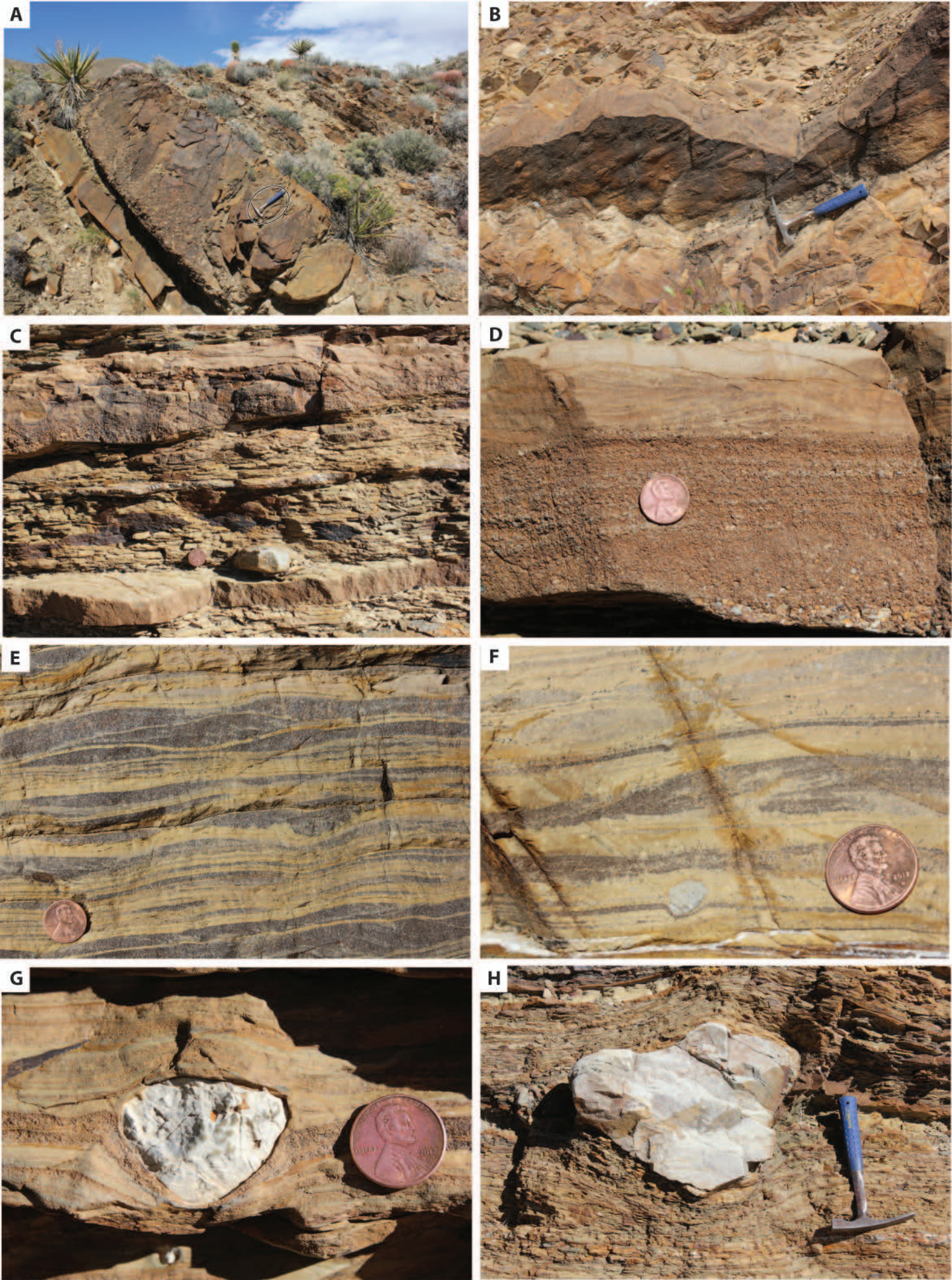
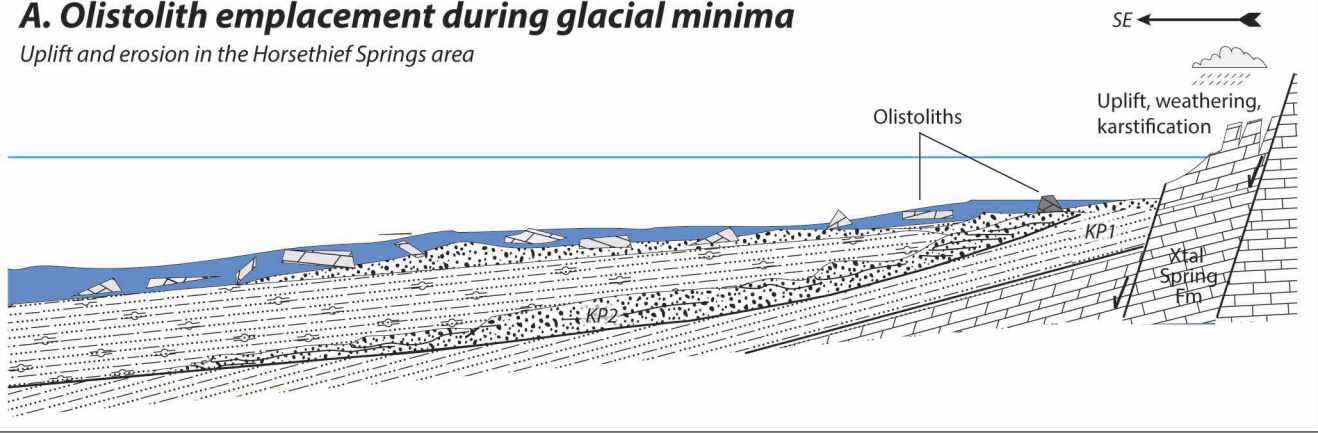


Figure 5

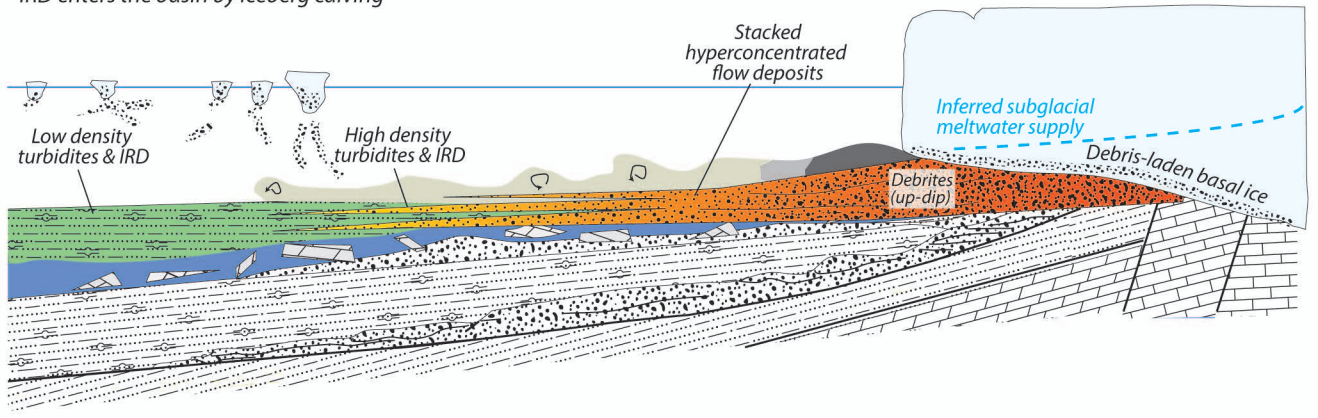
A. Olistolith emplacement during glacial minima

Uplift and erosion in the Horsethief Springs area



B. Prolific iceberg calving in a glacial re-advance

IRD enters the basin by iceberg calving



C. Cessation of iceberg calving in a glacial re-advance

Delivery of IRD to the basin arrested

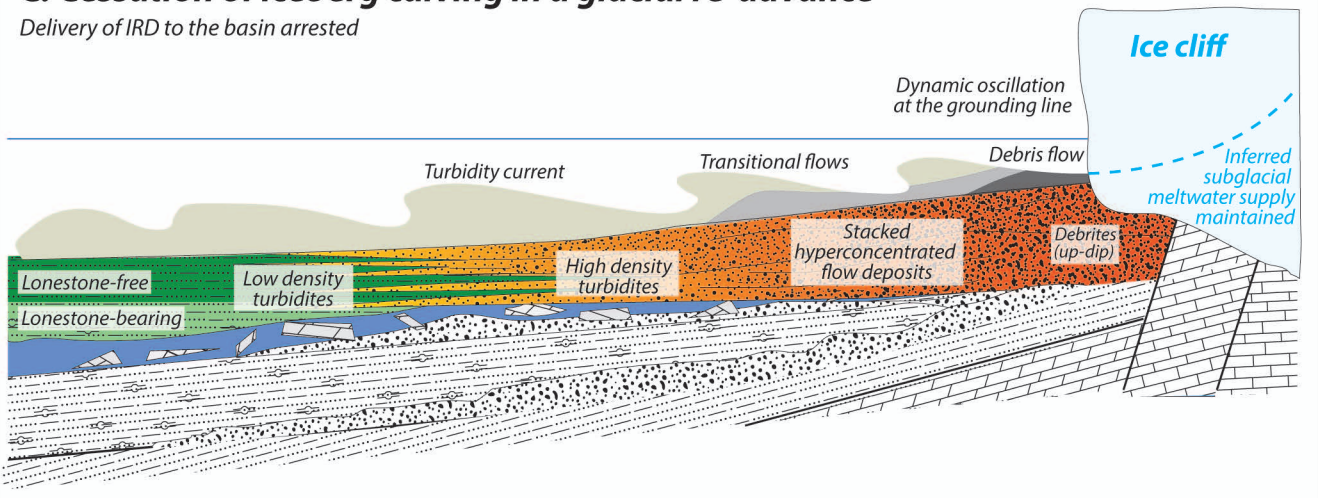


Figure 6

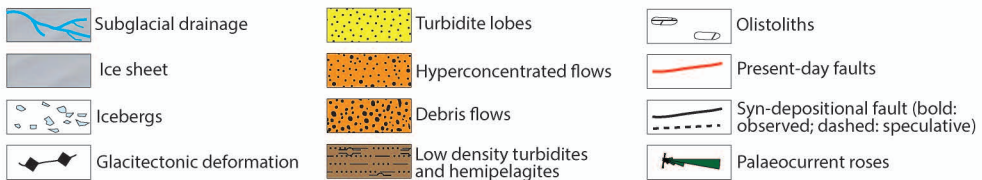
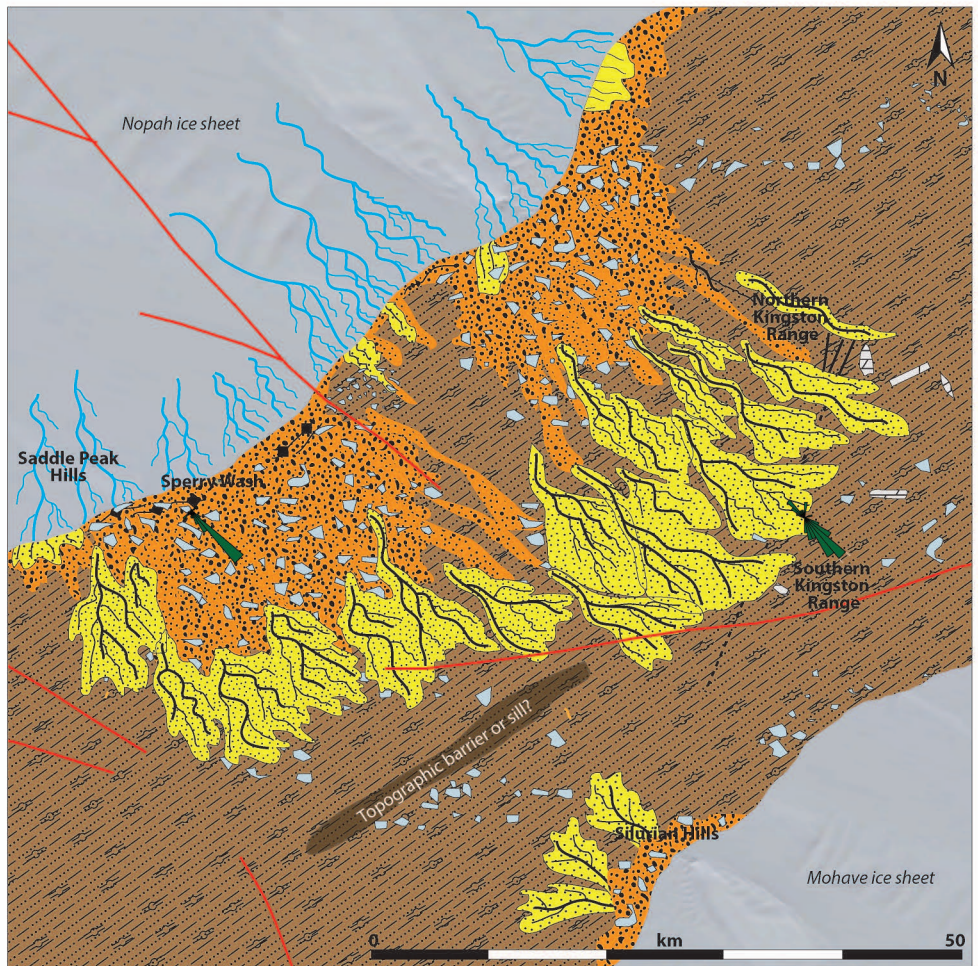


Figure 7